

OPEN ACCESS

EDITED BY Weisi Yan, University of Kentucky, United States

REVIEWED BY
Damodar Pokhrel,
University of Kentucky, United States
Alejandro Prado,
HM University Sanchinarro Hospital, Spain

*CORRESPONDENCE
Christine V. Chung
cchung2@mdanderson.org
Joshua S. Niedzielski
jsniedzielski@mdanderson.org

RECEIVED 05 August 2025 ACCEPTED 30 September 2025 PUBLISHED 31 October 2025

CITATION

Chung CV, Nair SS, Khan MS, Nguyen CI, Martin-Paulpeter RM, Ludmir EB, Court LE and Niedzielski JS (2025) Novel volumetric modulated arc therapy approach for lattice radiation therapy for bulky liver tumors. *Front. Oncol.* 15:1680342. doi: 10.3389/fonc.2025.1680342

COPYRIGHT

© 2025 Chung, Nair, Khan, Nguyen, Martin-Paulpeter, Ludmir, Court and Niedzielski. This is an open-access article distributed under the terms of the Creative Commons Attribution License (CC BY). The use, distribution or reproduction in other forums is permitted, provided the original author(s) and the copyright owner(s) are credited and that the original publication in this journal is cited, in accordance with accepted academic practice. No use, distribution or reproduction is permitted which does not comply with these terms.

Novel volumetric modulated arc therapy approach for lattice radiation therapy for bulky liver tumors

Christine V. Chung^{1*}, Saurabh S. Nair¹, Meena S. Khan¹, Callistus I. Nguyen¹, Rachael M. Martin-Paulpeter¹, Ethan B. Ludmir², Laurence E. Court¹ and Joshua S. Niedzielski^{1*}

¹Department of Radiation Physics, The University of Texas MD Anderson Cancer Center, Houston, TX, United States, ²Department of Gastrointestinal Radiation Oncology, The University of Texas MD Anderson Cancer Center, Houston, TX, United States

Purpose: Lattice radiation therapy (LRT) is a type of spatially fractionated radiation therapy that has emerged as an effective treatment approach for bulky solid tumors. RapidArc Dynamic (RAD) is a novel beam delivery approach that may be advantageous for LRT. The purpose of this *in silico* study was to evaluate and compare a novel RAD-based LRT approach (RAD-LRT) with conventional volumetric modulated arc therapy (VMAT)-based LRT (VMAT-LRT).

Methods: Twenty patients with bulky liver tumors treated with RT were retrospectively identified. VMAT-LRT and RAD-LRT plans were generated for all patients. Lattice spheres were placed in a standardized hexagonal pattern with alternating high-dose spheres (vertex tumor volume high [VTVH], analogous to the peak dose) and low-dose control spheres (vertex tumor volume low [VTVL], analogous to the valley dose). Gross tumor volumes (GTVs)<1,000 cm³ and GTVs \geq 1,000 cm³ were planned with 1.0-cm-diameter spheres (n=10) and 1.5-cm-diameter sphere (n=10), respectively. A prescription dose of 20 Gy to 80% of the VTVH was utilized. LRT dose metrics (e.g., peak-to-valley dose ratios, VTVH D80, VTVL D_{mean}) were calculated and were compared using paired Wilcoxon sign-ranked test. Planning efficiency was assessed by evaluating planning structures, planning time, and number of treatment fields.

Results: For all 20 cases, RAD-LRT achieved superior plan quality than VMAT-LRT, indicated by similar prescription dose coverage (group mean, VTVH D80: 20.40 Gy for VMAT-LRT, 20.50 Gy for RAD-LRT) but significantly lower valley dose (group mean, VTVL mean dose: 3.40 Gy for VMAT-LRT, 2.20 Gy for RAD-LRT, p<0.0001). Compared to VMAT-LRT, RAD-LRT required fewer planning structures (mean \pm SD, 9 \pm 1 for VMAT-LRT, 4 \pm 1 for RAD-LRT), less planning time (26 \pm 8 min for VMAT-LRT, 18 \pm 11 min for RAD-LRT), and fewer treatment beams (5 \pm 1 arcs for VMAT-LRT, 1 arc with 4 \pm 1 static ports for RAD-LRT). RAD-

LRT also had significantly higher peak-to-valley dose ratios (group mean, VTVH/ VTVL D90 ratio: 8.92 for VMAT-LRT, 18.20 for RAD-LRT, p<0.0001).

Conclusion: RAD may offer a unique approach to Lattice RT. RAD-LRT generated high quality plans with notable treatment planning efficiency, allowing for creation of quality plans without extensive planning time and LRT expertise.

KEYWORDS

spatially fractionated radiation therapy, lattice radiation therapy, VMAT, RapidArc Dynamic, liver cancer, hepatic cancer, bulky tumors, peak-to-valley dose ratio

1 Introduction

The evolution of radiation therapy, spurred by recent advances in technology and automation, continues to drive the exploration of innovative dose delivery strategies and treatment approaches. The management of large, bulky tumors remains complex, where maximizing tumor control and minimizing normal tissue toxicity can often make treatment planning both technically demanding and time intensive. Extensive liver tumors are a particular challenge due to proximity to organs at risk (OARs) (1–5). The pursuit of more effective and less toxic radiation therapy for large tumors has led to the exploration of spatially fractionated radiation therapy (SFRT) dose delivery techniques as a promising strategy for tumor debulking without increasing dose to normal tissues (5, 6). Although SFRT has existed for nearly a century, it was not until 2010 that the concept was translated into a 3D approach, known as lattice radiotherapy (LRT) (6, 7).

LRT is characterized by its lattice-like dose pattern of alternating high-dose peaks and low-dose valleys. High-dose peaks not only destroy tumor cells but also have been shown to elicit tumor-specific immunogenic responses (7, 8). Adjacent low-dose valleys appear to serve as a facilitator of this latter effect by preserving tumor vasculature, thereby allowing for perfusion of immunogenic factors (7, 9, 10). Furthermore, the bystander effect allows for a synergy with the immunomodulatory effects of SFRT, as the high-dose peaks induce sufficient cancer cell killing to achieve tumor control, despite not irradiating the entire GTV to a large homogenous dose of radiation that would otherwise suppress or kill host immune cells (11–15).

Often, the most challenging part of treatment planning for LRT is achieving sufficiently low valleys (i.e., often 20–25% of the prescription dose) without compromising the prescription goal (7, 16, 17). LRT is typically delivered as a volumetric modulated arc therapy (VMAT) treatment. While VMAT offers higher conformality and lower delivery time than intensity-modulated RT (IMRT), VMAT induces a low-dose wash of the entire treatment field, which is a drawback in SFRT if a minimal valley dose is desired.

RapidArc Dynamic (RAD) is a novel treatment approach that has the ability to combine the benefits of VMAT and IMRT by

incorporating static angles within the treatment arc, allowing for enhanced modulation at strategic angles. Moreover, RAD allows for a dynamic collimator that is optimized alongside the treatment plan, which can increase conformality without requiring multiple arcs. These features suggest a potential advantage of RAD-based LRT (RAD-LRT) over VMAT-based LRT (VMAT-LRT). We investigated the feasibility and dosimetric implications of employing RAD for the delivery of LRT. Specifically, we compared RAD-LRT with VMAT-LRT in terms of fulfillment of plan objectives, normal tissue sparing, and the efficiency of treatment planning.

2 Materials and methods

Computed tomography (CT) scans (2.5 mm slice thickness) from 20 patients were utilized for this planning study and were selected to include a large range of unresected, bulky hepatic tumor volumes. All patients had been treated with conventional external beam RT during 2020-2024. Gross tumor volumes (GTVs) ranged from 552 cm³ to 2,578 cm³ and were used to divide the cases into 2 subgroups: those with GTV less than 1,000 cm³ (GTV_{<1000}; n=10) and those with GTV 1,000 cm³ or larger (GTV_{≥1000}; n=10), see Table 1 for details per case. A dosimetrist and medical physicist, both with multiple years of clinical experience, generated VMAT-LRT and RAD-LRT plans for each case, and dosimetric analysis and comparison was performed. All procedures were performed in compliance with the Declaration of Helsinki and institutional guidelines, and this study was approved by the Institutional Review Board of The University of Texas MD Anderson Cancer Center (IRB number RCR03-400), which waived the requirement for informed consent.

2.1 Lattice setup

Seventeen patients were originally treated with breath-hold motion management, with the remaining 3 receiving free-breathing treatments using the average CT scan generated from 4DCT simulation datasets (in which case, the GTV was delineated

TABLE 1 Case details.

| Case no. | V _{GTV} [cm ³] | $\frac{V_{GTV}}{V_{Liver}}$ | $rac{V_{VTVH}}{V_{GTV}}$ | Sphere diameter [cm] | No. of VTVH spheres | No. of VTVL spheres | No. of sphere layers | VMAT No. of | | RAD No. of | |
|-------------|--|-----------------------------|---------------------------|----------------------------|---------------------------|---------------------------|----------------------------|-------------|-------|------------|-------|
| | | | | | | | | Arcs | MUs | Arcs | MUs |
| 1 | 2578 | 85% | 1.20% | 1.5 | 18 | 22 | 5 | 5 | 14681 | 1 + 5SP | 14878 |
| 2 | 2202 | 59% | 1.10% | 1.5 | 15 | 17 | 5 | 5 | 16603 | 1 + 4SP | 14161 |
| 3 | 1938 | 74% | 0.80% | 1.5 | 9 | 15 | 5 | 4 | 12632 | 1 + 5SP | 9509 |
| 4 | 1872 | 44% | 1.00% | 1.5 | 11 | 15 | 3 | 5 | 13324 | 1 + 5SP | 16374 |
| 5 | 1584 | 40% | 0.60% | 1.5 | 6 | 10 | 3 | 5 | 10831 | 1 + 4SP | 11327 |
| 6 | 1549 | 35% | 0.70% | 1.5 | 7 | 15 | 3 | 5 | 9526 | 1 + 5SP | 13349 |
| 7 | 1434 | 58% | 0.90% | 1.5 | 8 | 14 | 3 | 5 | 12510 | 1 + 4SP | 15007 |
| 8 | 1271 | 47% | 0.60% | 1.5 | 5 | 12 | 2 | 5 | 8716 | 1 + 4SP | 13067 |
| 9 | 1196 | 57% | 0.80% | 1.5 | 6 | 10 | 3 | 5 | 9592 | 1 + 4SP | 11889 |
| 10 | 1066 | 46% | 0.60% | 1.5 | 4 | 6 | 3 | 5 | 7927 | 1 + 5SP | 11486 |
| 11 | 993 | 33% | 0.60% | 1 | 13 | 17 | 3 | 5 | 7927 | 1 + 5SP | 16446 |
| 12 | 936 | 41% | 0.60% | 1 | 10 | 12 | 3 | 4 | 11824 | 1 + 5SP | 13035 |
| 13 | 880 | 39% | 0.50% | 1 | 10 | 11 | 2 | 4 | 11824 | 1 + 6SP | 12824 |
| 14 | 786 | 35% | 0.50% | 1 | 8 | 18 | 3 | 5 | 12081 | 1 + 4SP | 10931 |
| 15 | 733 | 25% | 0.60% | 1 | 9 | 12 | 3 | 4 | 13626 | 1 + 5SP | 15741 |
| 16 | 713 | 36% | 0.40% | 1 | 6 | 12 | 3 | 4 | 8851 | 1 + 4SP | 9620 |
| 17 | 660 | 26% | 0.40% | 1 | 5 | 5 | 2 | 5 | 10544 | 1 + 3SP | 12701 |
| 18 | 635 | 36% | 0.40% | 1 | 4 | 8 | 2 | 5 | 11247 | 1 + 4SP | 14772 |
| 19 | 632 | 25% | 0.70% | 1 | 10 | 15 | 3 | 5 | 13320 | 1 + 3SP | 12427 |
| 20 | 552 | 16% | 0.40% | 1 | 6 | 8 | 2 | 4 | 7936 | 1 + 4SP | 11230 |

No., number; V_{GTV} , volume of GTV; V_{GTV}/V_{Liver} percent of total liver volume that is GTV; V_{VTVH}/V_{GTV} , proportion of GTV that is VTVH; VTVH, vertex tumor volume high; VTVL, vertex tumor volume low; VMAT, volumetric modulated arc therapy; RAD, rapid arc dynamic; SP, static ports.

using the maximum intensity projection scan). Original clinical OAR structures and GTVs were utilized for planning and evaluation. As these patients were originally treated with conventional RT, all LRT-related structures, including planning targets, were newly generated for this planning study. The majority of LRT contours were generated automatically using an in-house custom script designed to standardize the sphere placements and planning approach. To ensure a conformal distribution, lattice spheres were placed in an alternating pattern with alternating high-dose spheres (vertex tumor volume high [VTVH], analogous to the peak dose) and low-dose control spheres (vertex tumor volume low [VTVL], analogous to the valley dose) in 3D space, a method adapted from the LITE SABR M1 protocol (18). GTV_{<1000} cases were configured with 1.0-cm-diameter spheres with 4.0-cm sphere center-to-center (CTC) distance in the axial plane and 3.0cm CTC distance in the superior-inferior direction. $GTV_{\geq 1000}$ cases utilized 1.5-cm-diameter spheres spaced with 6.0-cm center-tocenter (CTC) distance in the axial plane and 3.0-cm CTC distance in the superior-inferior direction (19). The lattice arrangement for GTV_{>1000} cases is diagrammed in Figure 1.

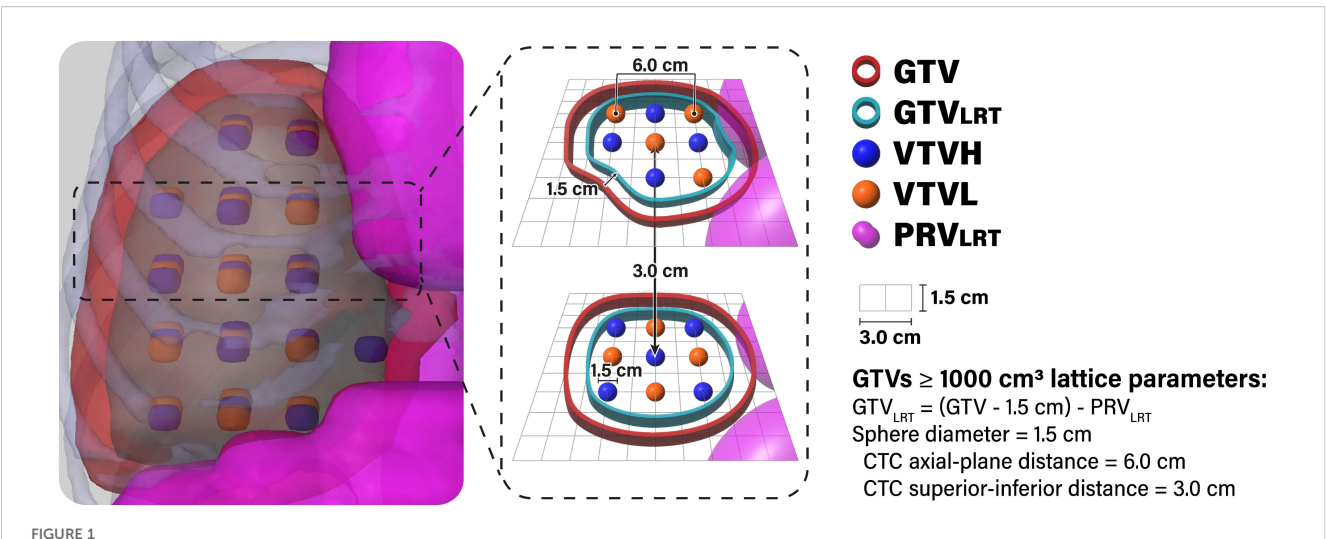
In order to determine the allowable region for placing VTVH spheres, the in-house custom script first generates a planning OAR

volume (PRV_{LRT}) through concatenation of all gastrointestinal luminal contours with an expansion of 1.0 cm for GTV_{<1000} cases and 1.5 cm for GTV_{≥1000} cases (7, 20, 21). Then, it creates the GTV_{LRT} by contracting the clinical GTV by 1.0 cm for GTV_{<1000} cases and 1.5 cm for GTV_{≥1000} cases and subtracting the PRV_{LRT} (Figure 1) (7, 22, 23). The script automatically removes whole VTVH spheres outside of the GTV_{LRT}, enabling optimal sparing of OARs and minimizing dose to the periphery of the GTV (7, 20–22). Whole VTVL spheres outside of the GTV are also removed.

2.2 Treatment planning

2.2.1 VMAT-LRT

VMAT-LRT plans were created following clinical workflow, using the RayStation treatment planning system (version 12A; RaySearch Laboratories, Stockholm, Sweden) and 5 \pm 1 flattening-filter-free 6-MV full arcs. Plans were generated on a TrueBeam linear accelerator (Varian Medical Systems, Palo Alto, CA) and dose calculations were performed with the collapsed cone algorithm. Collimator angles were chosen on the basis of the geometry of lattice spheres (Figure 2). Two arcs had collimator



Lattice arrangement for GTV $_{\geq 1000}$ cases. The GTV_{LRT} was created by contracting the GTV by 1.5 cm and subtracting the PRV_{LRT} (1.5-cm expansion of gastrointestinal luminal contours). Spheres alternated between high-dose spheres (VTVH) and low-dose spheres (VTVL) in all directions. VTVH and VTVL were both 1.5 cm in diameter and spaced with 6.0-cm CTC distance in the axial plane. An in-house custom script was used to automatically generate and place spheres and to remove VTVH outside of the GTV_{LRT} and VTVL outside of the GTV.

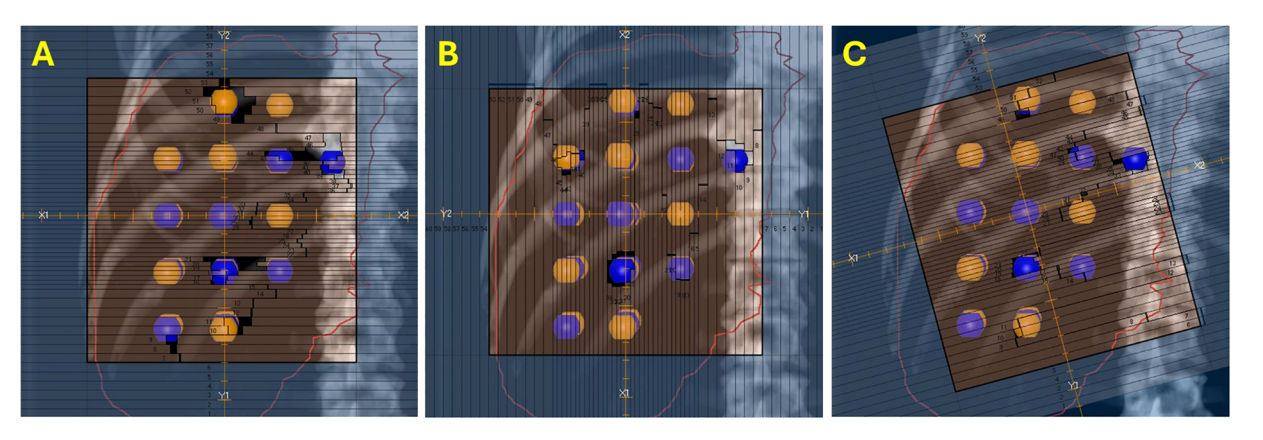


FIGURE 2
Collimator angles for VMAT-LRT. Blue, high-dose spheres (VTVH); orange, low-dose spheres (VTVL). (A, B) Collimator angles of 0°, 90°, or 270° for four out of five full arcs to optimize the modulation between lattice spheres. (C) One 15° off beam was also utilized to modulate around the spheres for a more conformal dose distribution.

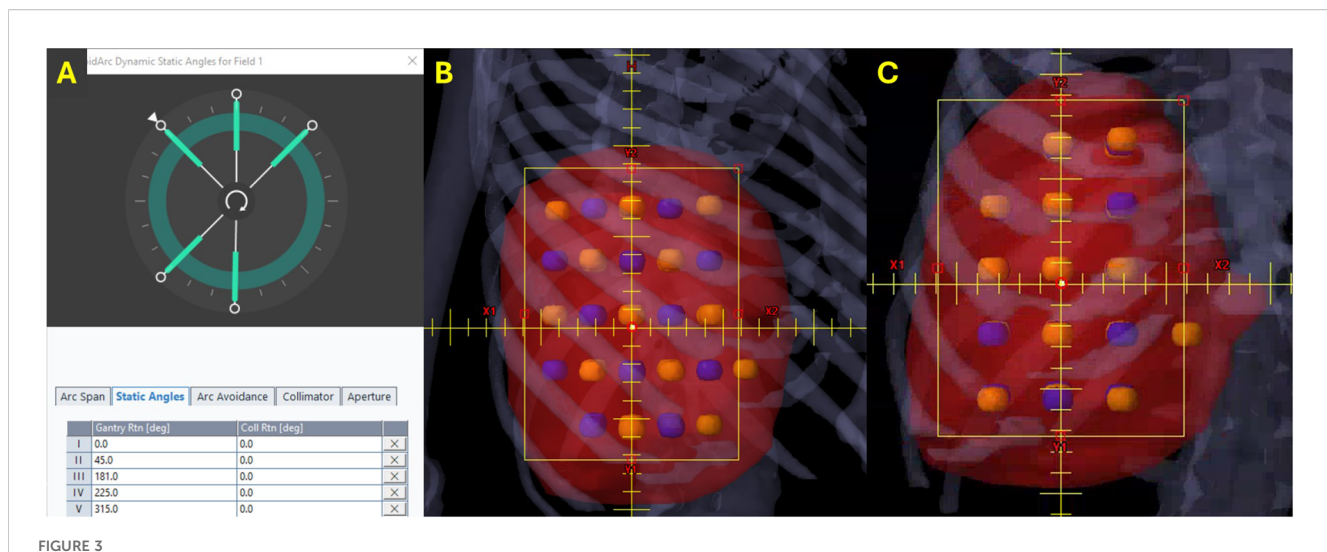
angles of 0°, two arcs had collimator angles of 90° or 270°, and one arc had a collimator angle of 15° off (15°, 315°, 30°, or 45°).

The majority of the VMAT planning structures were created using the same in-house custom script for consistency and efficiency, including fall-off rings (2–3 consecutive 5 mm rings) for the VTVH and VTVH, and structures to control max dose between sphere layers, and to the GTV periphery and normal tissue. Some cases required generating planning structures to control max dose to nearby OARs or hot or cold spots.

2.2.2 RAD-LRT

RAD-LRT plans were generated with the Eclipse treatment planning system, version 18.1 (Varian Medical Systems, Palo Alto, CA, USA), using a single flattening-filter-free 6-MV full arc.

Plans were generated on a TrueBeam linear accelerator (Varian Medical Systems, Palo Alto, CA) and calculated with the Acuros XB algorithm, version 18.1.0. RAD-LRT plans were generated using the same target and OAR structures used to generate the VMAT-LRT plans. RAD introduces a dynamic collimator, along with the ability to optimize collimator rotation throughout the arc; this feature was selected for the arc modulation between static fields. These static fields serve as ports, where the gantry rotation is paused during arc delivery to allow for more focused modulation, akin to IMRT fields. Applying the same logic as the VMAT-LRT plans, the static angles had a fixed 0° collimation to ensure modulation along the lattice (Figure 2A). Static angles were selected according to tumor location (proximity to skin surface or OARs) and sphere placement using the beams eye view (Figure 3). For all cases, the same 5 static angles



Static angles for RAD-LRT. Blue, high-dose spheres (VTVH); orange, low-dose spheres (VTVL). (A) All RAD cases were initially optimized with the same 5 static angles. (B) Three angles that capitalize on overlapping VTVH spheres without intersecting VTVL spheres (beams eye view). (C) Two angles that still modulate along the lattice but have VTVH and VTVL overlap (beams eye view).

TABLE 2 Lattice RT target volume objectives and constraints.

| Target volume | Target objectives | Constraint |
|---------------|-------------------------|-------------------------|
| GTV | D0.03cc< 25Gy | D0.03cc< 28Gy |
| VTVH | D80% ≥ 20Gy | D000/ > 20C- |
| VIVH | D90% ≥ 18Gy | D80% ≥ 20Gy |
| VTVL | D _{mean} ≤ 4Gy | D _{mean} ≤ 5Gy |

 $GTV, gross \ tumor \ volume; VTVH, vertex \ tumor \ volume \ high; VTVL, vertex \ tumor \ volume \ low.$

(0°, 45°, 181°, 225°, and 315°) were initially chosen, and then adjustments were made for each case (e.g., removed 181° for medial tumors to avoid the spinal cord, replaced 45° with 135° for right posterior targets) (Figure 3). The RAD optimizer allows for adjusting preference for modulation weighting between the arc sections and static angles, which are simultaneously optimized (24). All RAD-LRT cases were completed with balanced weighting between arc and static fields, which corresponds to 26 control points per port.

RAD-LRT plans were completed using a template, which included the following planning structures: normal tissue control, VTVL 5 mm expansion, VTVH 1.5 cm expansion, and a structure to control dose between sphere layers. Some cases required generating planning structures to control max dose to nearby OARs. Contouring hot or cold spots were not obviously necessary or beneficial for these cases, potentially due to RAD restarting optimization between runs (i.e., does not allow continuation of previous optimization) (24).

2.2.3 Plan objectives

The primary objective was delivery of 20 Gy in 1 fraction to 80% of the VTVH (the prescription dose); the secondary objective was delivery of a mean dose not exceeding 4 Gy to the VTVL (Table 2).

All lattice spheres were also kept as separate contours in the treatment planning system to allow for dose-volume histogram (DVH) visualization of each sphere to ensure adequate target coverage and minimal dose to the VTVL. Dose constraints for OARs, including the uninvolved liver, kidneys, stomach, duodenum, heart, and spinal cord, were based on institutional protocols or guidelines (Table 3).

2.3 Plan review and statistical analyses

All final plans were reviewed by a dosimetrist and a medical physicist, both knowledgeable in VMAT-LRT and RAD-LRT planning. The peak volume (VTVH) was defined as the concatenation of all high-dose vertices. The valley volume (VTVL) was defined as the concatenation of all low-dose vertices. The maximum doses delivered to 5%, 10%, 20%, 50%, 80%, 90%, 95%, and 100% of the target volume (D5%, D10%, D20%, D50%, D80%, D90%, D95%, and D100%, respectively), along with the mean dose and max dose (D0.03cc), were assessed for VTVH and VTVL for all VMAT-LRT and RAD-LRT plans. The authors proposed and evaluated a surrogate equation to calculate peak-to-valley dose ratios (PVDRs). As the goal is to evaluate the overall target dose heterogeneity, the ratio of the near max (D90%) of the peak (VTVH) dose and the near min (D90%) of the valley (VTVL) dose was selected for the definition of PVDR for this study.

PVDR was defined by the following formula:

$$\mathbf{PVDR} = \frac{D90 \% \text{ VTVH}}{D90 \% \text{ VTVL}}$$

The max dose was recorded for the tissue 1.0 cm outside of the GTV and for the PRV_{LRT} to assess normal tissue sparing. A paired Wilcoxon signed-rank test was used for comparison of all LRT dose metrics, with statistical significance determined using a Bonferroni-

TABLE 3 Lattice RT OAR objectives and constraints.

| Structure | OAR objectives | Constraint | |
|-------------|--------------------------|------------------------------|--|
| Spinal cord | D0.03cc< 6 Gy | D0.03cc< 6 Gy | |
| Esophagus | D0.03cc< 6 Gy | ALARA | |
| Heart | D0.03cc< 6 Gy | ALARA | |
| Stomach | D0.03cc< 6 Gy | ALARA | |
| Duodenum | D0.03cc< 6 Gy | ALARA | |
| Rt kidney | V7Gy< 67% | ALARA | |
| Lt kidney | V7Gy< 67% | ALARA | |
| Kidneys | D _{mean} < 7 Gy | D _{mean} < 12.50 Gy | |
| Liver-GTV | D700cc (ALARA) | V20Gy< 700 cc | |
| Small bowel | D0.03cc< 6 Gy | ALARA | |
| Large bowel | D0.03cc< 6 Gy | ALARA | |
| Rectum | D0.03cc< 6 Gy | ALARA | |
| Bladder | D0.03cc< 6 Gy | ALARA | |

ALARA, as low as reasonably achievable; D700cc, maximum dose delivered to 700 cc of the target volume; V7Gy, volume receiving at least 7 Gy; V20Gy, volume receiving at least 20 Gy.

adjusted threshold of p< 0.0016 (0.05/31 comparisons) to reduce the risk of Type I errors for multiple comparisons. All statistical analyses were performed using RStudio (version 4.2.1; Posit Software; Boston, Massachusetts).

In addition to being evaluated in terms of dose statistics, each treatment planning approach was evaluated in terms of efficiency in treatment planning, specifically planning time (i.e., optimization time and additional planning structure generation (structures not

generated by in-house script)), and number of beams and planning structures.

3 Results

3.1 Dose statistics

Figure 4 shows a representative comparison of the dose distributions and DVH for the VMAT-LRT and RAD-LRT plans, for case 4 (see Table 1 for case details). The figure demonstrates the benefit of RAD in minimizing 5 Gy to centroid VTVL spheres without reduction in surrounding VTVH coverage or conformality.

All VMAT-LRT and RAD-LRT plans met the OAR constraints and target objectives (Table 4). VMAT-LRT and RAD-LRT plans met the target prescription of D80% ≥20 Gy (Table 4, Figure 5A, B); however, RAD-LRT plans had significantly higher D90%, D95%, and D100% values, indicating higher target conformality (Table 4, Figure 5C). Across all DVH statistics, the VTVL doses were significantly lower with RAD-LRT than with VMAT-LRT (Table 4, Figure 5D, E). PVDRs were significantly higher for RAD-LRT (Table 4, Figure 5F), when compared to VMAT_LRT, indicating higher achieved dose heterogeneity. Figure 6 shows PVDR achieved for each case's VMAT-LRT and RAD-LRT plans.

Sparing of the normal tissue 1.0 cm outside of the GTV was similar for VMAT-LRT and RAD-LRT; however, the PRV_{LRT} received a significantly lower maximum dose in the RAD-LRT plans (Table 4). VMAT-LRT and RAD-LRT produced similar levels of sparing of the liver minus GTV, although RAD-LRT showed a slight advantage.

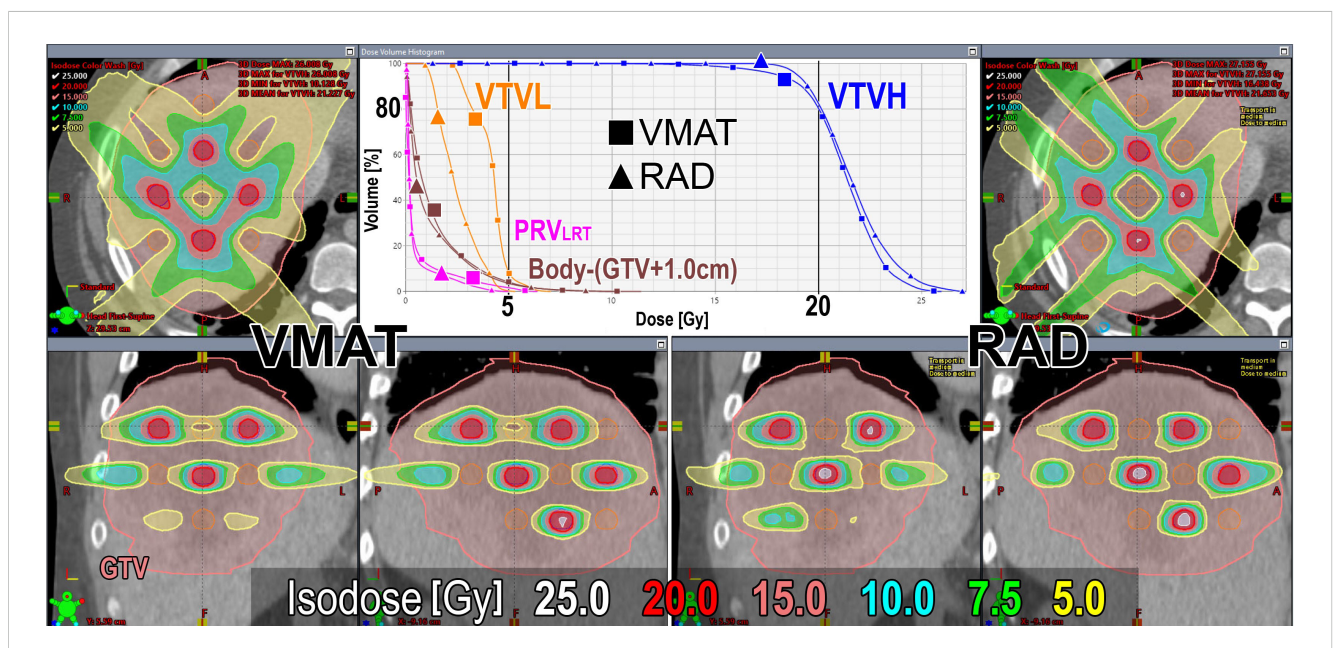
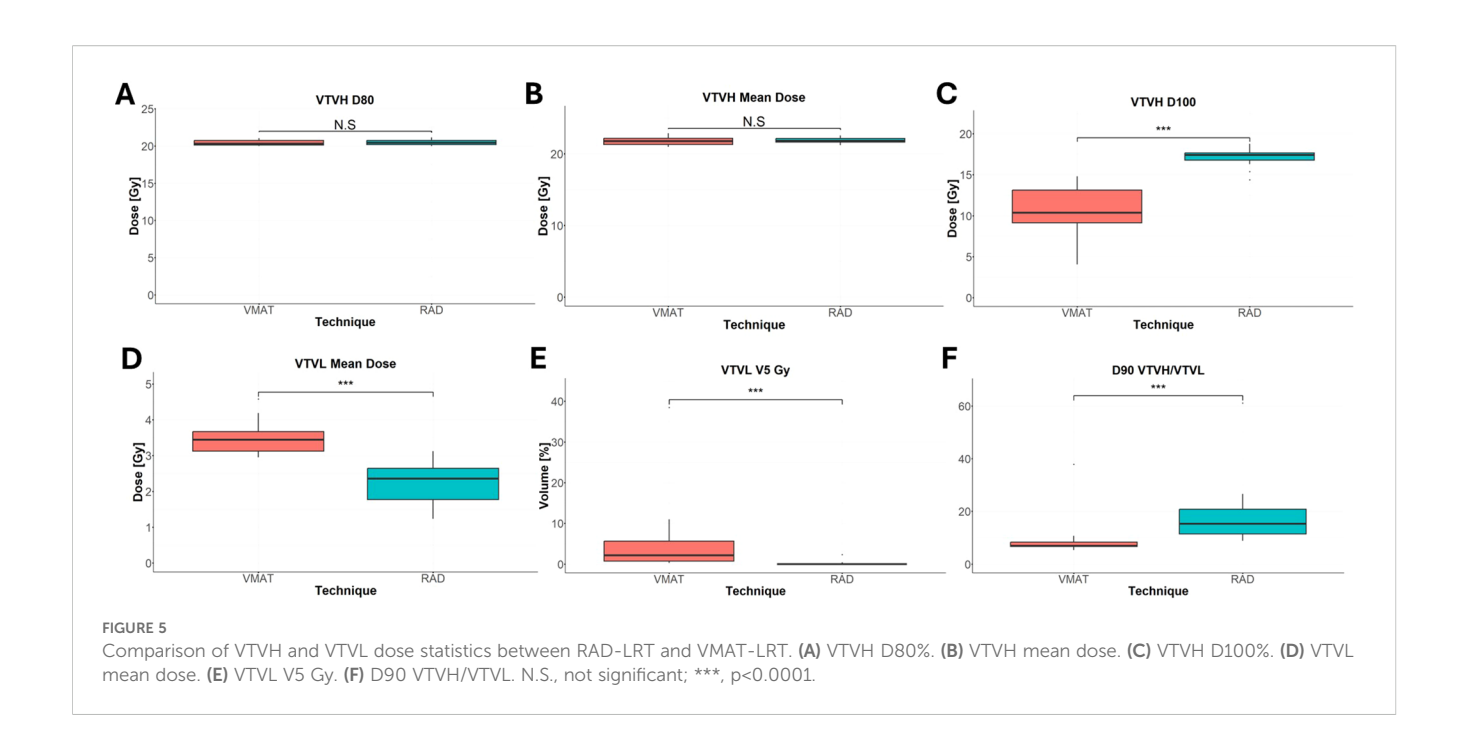


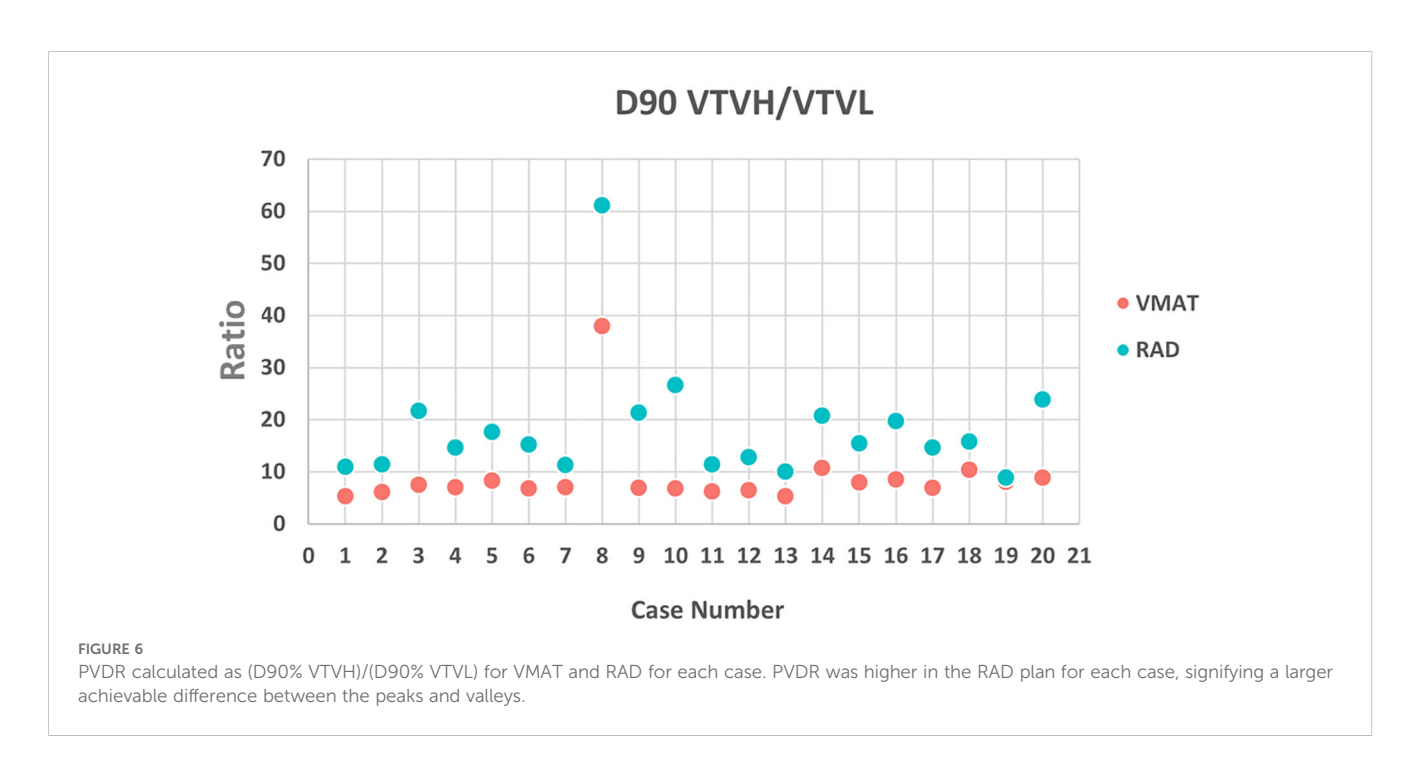
FIGURE 4
Dose distributions and DVH comparison of VMAT (left/square) and RAD (right/triangle) plans for case 4 (case details in Table 1). GTV is contoured in pink, VTVL (low-dose spheres) is contoured in orange, and VTVH (high-dose spheres) is contoured in blue. Prescription is D80% >20 Gy in 1 fraction.

TABLE 4 Dose-volume histogram metrics for VMAT and RAD.

| Metric | Median (range) [Gy] | VMAT group mean [Gy] | RAD group mean [Gy] | P-value | | | |
|-----------------|----------------------|----------------------|---------------------|----------|--|--|--|
| | | VTVH | | | | | |
| Mean Dose | 21.83 (20.98-23.44) | 21.70 | 21.90 | 0.16 | | | |
| D5% | 24.69 (23.46-26.54) | 24.80 | 24.50 | 0.09 | | | |
| D10% | 24.14 (23.00-25.81) | 24.20 | 24.00 | 0.11 | | | |
| D20% | 23.44 (22.37-25.10) | 23.50 | 23.30 | 0.08 | | | |
| D50% | 21.92 (21.12-23.36) | 22.00 | 23.30 | 0.21 | | | |
| D80% | 20.48 (20.00-21.87) | 20.40 | 20.50 | 0.38 | | | |
| D90% | 19.41 (11.76-21.32) | 18.80 | 20.00 | <0.0001* | | | |
| D95% | 18.29 (8.29-20.88) | 17.00 | 19.50 | <0.0001* | | | |
| D100% | 13.89 (4.05-18.77) | 10.60 | 17.10 | <0.0001* | | | |
| D0.03cc | 25.77 (24.30-27.38) | 25.90 | 25.60 | 0.14 | | | |
| VTVL | | | | | | | |
| Mean Dose | 2.86 (1.23-4.58) | 3.40 | 2.20 | <0.0001* | | | |
| D5% | 4.20 (2.14-7.47) | 4.80 | 3.50 | <0.0001* | | | |
| D10% | 3.87 (1.96-6.13) | 4.40 | 3.30 | <0.0001* | | | |
| D20% | 3.52 (1.63-5.78) | 4.10 | 2.90 | <0.0001* | | | |
| D50% | 2.80 (1.09-4.42) | 3.40 | 2.20 | <0.0001* | | | |
| D80% | 2.16 (0.41-3.68) | 2.70 | 1.60 | <0.0001* | | | |
| D90% | 1.90 (0.32-3.30) | 2.40 | 1.30 | <0.0001* | | | |
| D95% | 1.71 (0.28-3.08) | 2.20 | 1.10 | <0.0001* | | | |
| D100% | 1.23 (0.21-2.33) | 1.60 | 0.80 | <0.0001* | | | |
| D0.03cc | 5.00 (2.50-9.18) | 5.80 | 4.10 | <0.0001* | | | |
| V5 Gy | 2.50% (0.00%-38.00%) | 5.00% | 0.15% | <0.0001* | | | |
| | | Body-(GTV + 1.0cm) | | | | | |
| D0.03cc | 8.57 (5.64-10.85) | 8.20 | 8.90 | 0.98 | | | |
| | | PRV _{LRT} | | | | | |
| D0.03cc | 8.18 (3.35-20.16) | 9.67 | 6.70 | <0.0001* | | | |
| | | VTVH/VTVL | | | | | |
| D50% | 9.12 (4.79-31.19) | 6.52 | 11.72 | <0.0001* | | | |
| D80% | 12.09 (5.47-49.24) | 8.57 | 15.61 | <0.0001* | | | |
| D90% | 13.58 (5.31-61.06) | 8.92 | 18.20 | <0.0001* | | | |
| D100% | 16.57 (1.73-78.04) | 7.77 | 25.37 | <0.0001* | | | |
| Liver minus GTV | | | | | | | |
| Mean Dose | 1.17 (0.5-2.43) | 1.21 | 1.13 | <0.05 | | | |
| D700cc | 0.70 (0-2.25) | 0.77 | 0.64 | <0.001 | | | |
| D0.03cc | 9.14 (6.47-13.88) | 9.40 | 8.88 | 0.18 | | | |
| Max Dose | 9.63 (6.88-14.75) | 9.95 | 9.30 | 0.10 | | | |

VTVH, vertex tumor volume high; VTVL, vertex tumor volume low; PRV_{LRT} , GI luminal contours with a 1.0–1.5 cm (GTV<1000 and GTV≥1000 respectively) expansion; VMAT, volumetric modulated arc therapy; RAD, rapid arc dynamic; Body-(GTV + 1.0cm), Body contour minus GTV with a 1.0 cm margin. *p<0.0016 – Statistical significance determined using a Bonferroni-adjusted threshold.





3.2 Planning efficiency

RAD was generally efficient for creating quality LRT plans. RAD-LRT plans required fewer planning structures (9 \pm 1 for VMAT-LRT, 4 \pm 1 for RAD-LRT), less planning time (26 \pm 8 min for VMAT-LRT, 18 \pm 11 min for RAD-LRT), and fewer treatment beams (5 \pm 1 arcs for VMAT-LRT, 1 arc with 4 \pm 1 static ports for RAD-LRT). In addition, all RAD-LRT cases followed the same planning template and steps, with only 2 plans requiring further

editing of optimization objectives, suggesting that RAD-LRT requires minimal customization between cases.

4 Discussion

This study showed that there is a significant advantage to using RAD over standard VMAT for LRT, which is a widely adopted SFRT approach. The novel components of RAD, specifically the

optimized dynamic collimator rotation and increased modulation at strategically selected static gantry angles, mitigate many of the inherent complexities traditionally associated with treatment planning for LRT [i.e., the required dose heterogeneity to treat target with high enough cancer-killing dose while also achieving low enough valley dose to spare channels of tissue between target spheres (7, 16, 17)]. This is the first study to compare the dosimetry of RAD and VMAT for LRT treatment planning.

The advantages of utilizing RAD for LRT were observed across a wide array of bulky liver tumors with a dataset of GTVs ranging from 552 cm³ (16% of the whole liver) to 2,578 cm³ (85% of the whole liver) (Tables 1, 4). This range of GTVs allowed for comprehensive testing and comparison, in line with previous studies (7, 22). Primarily, RAD appears to be better able to modulate the dose between separated targets, thus allowing for both more conformal VTVH (high-dose/peak spheres) and significantly reduced dose to the VTVL (low-dose/valley spheres) (Table 4, Figure 5). In LRT, reducing valley doses below 5 Gy is desirable if the treatment goal is tumor debulking through synergy of tumor-killing and immunomodulatory effects, as a dose below 5 Gy retains adequate perfusion of immune cells (4, 7, 22, 25, 26). The mean proportion of the VTVL receiving ≤5 Gy was 5% for VMAT but just 0.1% for RAD (Table 4). Rivera et al. (27) and Fernandez-Palomo et al. (28) both showed that in SFRT, the correlation between valley minimum and treatment response was stronger than the correlation between peak dose and treatment response, which emphasizes the importance of the significantly lower doses to the VTVL that RAD is able to achieve. The use of VTVL spheres, which were systematically placed along the lattice between the VTVH spheres, ensured even distribution of channels of intact perfusion throughout the tumor while maintaining the global geometric structure (18).

Of note, the lattice and vertices were automatically generated using an in-house script, which standardized the LRT setup and planning approach for all cases. Zhang et al. emphasized the importance of standardization of LRT not only for patient care but also for comparability of clinical trials and outcome results (5). Tucker et al. (29) and Gaudreault et al. (30) showed promising results with script-based algorithms to generate LRT lattice structures; both groups showed reduced dependency on user experience for sphere placement and hands-on planning time. Gaudreault et al. found that a fixed lattice geometry was not suitable for all patients (31), and in their follow-up study, they found that optimal lattice geometry can be estimated on the basis of tumor volume (30). As such, our script was designed with the option of generating lattice geometry for tumor volumes smaller than 1,000 cm³ or 1,000 cm³ or larger (details in Section 2.1), and can be further customized for variable lattice size or CTC distance.

While there is a general consensus on the need to evaluate the PVDR for LRT plans, exactly how to calculate this metric has been an ongoing topic of discussion (5, 21, 32, 33). Supplementary Figure S1 depicts VMAT-LRT and RAD-LRT comparison using other common PVDR definitions. Since our goal was to systematically minimize valley dose between peaks, we incorporated low-dose

valley spheres as avoidance structures rather than a "GTV minus high-dose spheres" volume. Given this approach, we utilized a PVDR surrogate metric of (D90% VTVH)/(D90% VTVL). This summary metric is in line with the theory behind the Radiosurgery Society white paper recommendation to use D90/D10 (i.e., VPDR) as single point doses may not accurately represent plan quality (5). The RAD plans in our study had significantly higher PVDR than the VMAT plans had, signifying that RAD was able to achieve a larger difference between the peaks and valleys, with the bulk of the difference due to the lower VTVL dose (Table 4, Figures 5, 6).

Although proton and carbon ion therapies have also shown lower valley doses than VMAT (34, 35), photon RT is more widely accessible. RAD offers an alternative form of photon radiation delivery through software update (Eclipse version 18.1; Varian Medical Systems, Palo Alto, CA) and utilization of existing hardware (TrueBeam 4.1; Varian Medical Systems, Palo Alto, CA) and therefore is more readily accessible than proton or heavy-ion SFRT at this time.

A limitation of this study is that while we have access to the planning portion of RAD treatment, we do not currently have a method to validate through machine delivery and measurement, so it was not possible to determine if these plans are deliverable as currently created. Continued research on validation and deliverability of these plans would be interesting, as well as further exploration of other treatment sites. As the plans were completed in different treatment planning systems that utilize different calculation algorithms, further research should be done to validate results using the same system. However, it should be noted that both VMAT-LRT and RAD-LRT plans used currently standard of care treatment planning systems and the most common clinically utilized dose calculation algorithms. Another limitation is that it is difficult to directly compare the results of this study with results of other studies, as there is little standardization in lattice treatment and plan metric reporting at this time (7).

Lastly, for almost all RAD plans, the planning goals were met with use of only a planning template, and only 2 plans required customization, suggesting that less experience may be required to generate a quality RAD-LRT plan than to generate a quality VMAT-LRT plan. Further research into standardization through automated plan setup and treatment planning could be useful as LRT becomes more mainstream.

5 Conclusion

In this study, an LRT planning approach utilizing a custom inhouse script to generate the lattice spheres was used to generate plans for 2 photon dose delivery methods, VMAT and RAD. RAD-LRT showed high plan quality, as indicated by comparable target coverage but lower valley doses when compared to conventional VMAT-LRT treatment plans. RAD-LRT also demonstrated high treatment planning efficiency, suggesting that RAD may offer a unique approach to planning this complex SFRT modality.

Data availability statement

The raw data supporting the conclusions of this work will be made available upon reasonable request and commensurate with a valid data sharing agreement with MD Anderson Cancer Center.

Ethics statement

The studies involving humans were approved by IRB of the MD Anderson Cancer Center (IRB no.: RCR03-0400). The studies were conducted in accordance with the local legislation and institutional requirements. Written informed consent for participation was not required from the participants or the participants' legal guardians/next of kin in accordance with the national legislation and institutional requirements. Written informed consent was obtained from the individual(s) for the publication of any potentially identifiable images or data included in this article.

Author contributions

CC: Data curation, Formal analysis, Investigation, Methodology, Validation, Visualization, Writing – original draft, Writing – review & editing. SN: Data curation, Formal analysis, Software, Writing – original draft, Writing – original draft, Writing – review & editing. MK: Data curation, Investigation, Writing – original draft, Writing – review & editing. CN: Software, Writing – original draft, Writing – review & editing. RM: Data curation, Methodology, Writing – original draft, Writing – review & editing. EL: Conceptualization, Methodology, Writing – original draft, Writing – review & editing. LC: Conceptualization, Funding acquisition, Writing – original draft, Writing – review & editing. JN: Conceptualization, Data curation, Investigation, Methodology, Project administration, Resources, Supervision, Validation, Writing – original draft, Writing – review & editing.

Funding

The author(s) declare financial support was received for the research and/or publication of this article. Varian provided funding for this work, which utilized their product as the primary tool under investigation (RapidArc Dynamic).

References

- 1. Tubin S, Popper HH, Brcic L. Novel stereotactic body radiation therapy (SBRT)-based partial tumor irradiation targeting hypoxic segment of bulky tumors (SBRT-PATHY): improvement of the radiotherapy outcome by exploiting the bystander and abscopal effects. *Radiat Oncol.* (2019) 14:21. doi: 10.1186/s13014-019-1227-y
- 2. Crane CH, Koay EJ. Solutions that enable ablative radiotherapy for large liver tumors: fractionated dose painting, simultaneous integrated protection, motion management and CT image guidance. *Cancer*. (2016) 122:1974–86. Available online at: https://www.ncbi.nlm.nih.gov/pmc/articles/PMC4911237/.

Acknowledgments

Editorial support was provided by Stephanie Deming, Senior Scientific Editor, Research Medical Library at MD Anderson Cancer Center.

Conflict of interest

CC, SN, CN, MK, LC, and JN all report funding from Varian Medical Systems.

The remaining authors declare that the research was conducted in the absence of any commercial or financial relationships that could be construed as a potential conflict of interest.

Generative AI statement

The author(s) declare that no Generative AI was used in the creation of this manuscript.

Any alternative text (alt text) provided alongside figures in this article has been generated by Frontiers with the support of artificial intelligence and reasonable efforts have been made to ensure accuracy, including review by the authors wherever possible. If you identify any issues, please contact us.

Publisher's note

All claims expressed in this article are solely those of the authors and do not necessarily represent those of their affiliated organizations, or those of the publisher, the editors and the reviewers. Any product that may be evaluated in this article, or claim that may be made by its manufacturer, is not guaranteed or endorsed by the publisher.

Supplementary material

The Supplementary Material for this article can be found online at: https://www.frontiersin.org/articles/10.3389/fonc.2025.1680342/full#supplementary-material

- 3. Bujold A, Massey CA, Kim JJ, Brierley J, Cho C, Wong RKS, et al. Sequential phase I and II trials of stereotactic body radiotherapy for locally advanced hepatocellular carcinoma. *J Clin Oncol.* (2013) 31:1631–9. doi: 10.1200/JCO.2012.44.1659
- 4. Ahmed MM, Wu X, Mohiuddin M, Perez NC, Zhang H, Amendola BE, et al. Optimizing GRID and lattice spatially fractionated radiation therapy: innovative strategies for radioresistant and bulky tumor management. *Semin Radiat Oncol.* (2024) 34:310–22. Available online at: https://linkinghub.elsevier.com/retrieve/pii/S1053429624000304 (Accessed June 6, 2025).

- 5. Zhang H, Wu X, Zhang X, Chang SX, Megooni A, Donnelly ED, et al. Photon GRID radiation therapy: A physics and dosimetry white paper from the radiosurgery society (RSS) GRID/LATTICE, microbeam and FLASH radiotherapy working group. *Radiat Res.* (2020) 194:665–677. doi: 10.1667/RADE-20-00047.1.full
- 6. Wu X, Ahmed MM, Wright J, Gupta S, Pollack A. On modern technical approaches of three-dimensional high-dose lattice radiotherapy (LRT). *Cureus*. (2010) 2:e9. Available online at: http://www.cureus.com/papers/13 (Accessed June 6, 2025).
- 7. Wu X, Perez NC, Zheng Y, Li X, Jiang L, Amendola BE, et al. The technical and clinical implementation of lattice radiation therapy (LRT). *Radiat Res.* (2020) 194:737–746. doi: 10.1667/RADE-20-00066.1.full
- 8. Lee Y, Auh SL, Wang Y, Burnette B, Wang Y, Meng Y, et al. Therapeutic effects of ablative radiation on local tumor require CD8+ T cells: changing strategies for cancer treatment. *Blood.* (2009) 114:589–95. Available online at: https://ashpublications.org/blood/article/114/3/589/131348/Therapeutic-effects-of-ablative-radiation-on-local (Accessed June 6, 2025).
- 9. Liang H, Deng L, Chmura S, Burnette B, Liadis N, Darga T, et al. Radiation-induced equilibrium is a balance between tumor cell proliferation and T cell–mediated killing. *J Immunol*. (2013) 190:5874–81. Available online at: https://journals.aai.org/jimmunol/article/190/11/5874/86914/Radiation-Induced-Equilibrium-Is-a-Balance-between (Accessed June 6, 2025).
- 10. Martinez-Zubiaurre I, Chalmers AJ, Hellevik T. Radiation-induced transformation of immunoregulatory networks in the tumor stroma. *Front Immunol.* (2018) 9:1679/full. doi: 10.3389/fimmu.2018.01679/full
- 11. Mohiuddin M, Park H, Hallmeyer S, Richards J. High-dose radiation as a dramatic, immunological primer in locally advanced melanoma. *Cureus.* (2015). Available online at: http://www.cureus.com/articles/3938-high-dose-radiation-as-a-dramatic-immunological-primer-in-locally-advanced-melanoma.
- 12. Kanagavelu S, Gupta S, Wu X, Philip S, Wattenberg MM, Hodge JW, et al. *In vivo* effects of lattice radiation therapy on local and distant lung cancer: potential role of immunomodulation. *Radiat Res.* (2014) 182:149–62. doi: 10.1667/RR3819.1
- 13. Hei TK, Zhou H, Ivanov VN, Hong M, Lieberman HB, Brenner DJ, et al. Mechanism of radiation-induced bystander effects: a unifying model. *J Pharm Pharmacol.* (2010) 60:943–50. Available online at: https://academic.oup.com/jpp/article/60/8/943/6147659 (Accessed June 6, 2025).
- 14. Chang MC, Chen YL, Lin HW, Chiang YC, Chang CF, Hsieh SF, et al. Irradiation Enhances Abscopal Anti-tumor Effects of Antigen-Specific Immunotherapy through Regulating Tumor Microenvironment. *Mol Ther.* (2018) 26:404–19. Available online at: https://linkinghub.elsevier.com/retrieve/pii/S1525001617305701 (Accessed June 6, 2025).
- 15. Tubin S, Yan W, Mourad WF, Fossati P, Khan MK. The future of radiation-induced abscopal response: beyond conventional radiotherapy approaches. *Future Oncol.* (2020) 16:1137–51. doi: 10.2217/fon-2020-0063
- 16. Zhang W, Lin Y, Wang F, Badkul R, Chen RC, Gao H. Lattice position optimization for lattice therapy. *Med Phys.* (2023) 50:7359–67. doi: 10.1002/mp.16572
- 17. Prezado Y, Lamirault C, Larcher T, Gilbert C, Espenon J, Patriarca A, et al. On the significance of peak dose in normal tissue toxicity in spatially fractionated radiotherapy: The case of proton minibeam radiation therapy. *Radiother Oncol.* (2025) 205:110769. Available online at: https://linkinghub.elsevier.com/retrieve/pii/S0167814025000647 (Accessed June 6, 2025).
- 18. Kavanaugh JA, Spraker MB, Duriseti S, Basarabescu F, Price A, Goddu M, et al. LITE SABR M1: Planning design and dosimetric endpoints for a phase I trial of lattice SBRT. *Radiother Oncol.* (2022) 167:172–8. Available online at: https://linkinghub.elsevier.com/retrieve/pii/S0167814021090460 (Accessed June 6, 2025).
- 19. Duriseti S, Kavanaugh J, Goddu S, Price A, Knutson N, Reynoso F, et al. Spatially fractionated stereotactic body radiation therapy (Lattice) for large tumors. *Adv Radiat Oncol.* (2021) 6:100639. Available online at: https://linkinghub.elsevier.com/retrieve/pii/S2452109420303699 (Accessed June 6, 2025).
- 20. Grams MP, Tseung HSWC, Ito S, Zhang Y, Owen D, Park SS, et al. A dosimetric comparison of lattice, brass, and proton grid therapy treatment plans. *Pract Radiat Oncol.* (2022) 12:e442–52. Available online at: https://linkinghub.elsevier.com/retrieve/pii/S1879850022000832 (Accessed June 6, 2025).

- 21. Grams MP, Owen D, Park SS, Petersen IA, Haddock MG, Jeans EB, et al. VMAT grid therapy: A widely applicable planning approach. *Pract Radiat Oncol.* (2021) 11: e339–47. Available online at: https://linkinghub.elsevier.com/retrieve/pii/S1879850020302617 (Accessed June 6, 2025).
- 22. Prado A, Martí J, García De Acilu P, Zucca D, Ángel de la Casa M, García J, et al. Dosimetrical and geometrical parameters in single-fraction lattice radiotherapy for the treatment of bulky tumors: Insights from initial clinical experience. *Phys Med.* (2024) 123:103408. Available online at: https://linkinghub.elsevier.com/retrieve/pii/S1120179724002035 (Accessed June 6, 2025).
- 23. Tubin S, Khan MK, Salerno G, Mourad WF, Yan W, Jeremic B. Monoinstitutional phase 2 study of innovative Stereotactic Body RadioTherapy targeting PArtial Tumor HYpoxic (SBRT-PATHY) clonogenic cells in unresectable bulky nonsmall cell lung cancer: profound non-targeted effects by sparing peri-tumoral immune microenvironment. *Radiat Oncol.* (2019) 14:212. doi: 10.1186/s13014-019-1410-1
- 24. Schroeder E. Eclipse TPS 18.1 New Features Workbook Palo Alto, CA: Varian Medical Systems. (2019).
- 25. Park HJ, Griffin RJ, Hui S, Levitt SH, Song CW. Radiation-induced vascular damage in tumors: implications of vascular damage in ablative hypofractionated radiotherapy (SBRT and SRS). *Radiat Res.* (2012) 177:311–27. doi: 10.1667/RR2773.1.full
- 26. Peng V, Suchowerska N, Esteves ADS, Rogers L, Claridge Mackonis E, Toohey J, et al. Models for the bystander effect in gradient radiation fields: Range and signalling type. *J Theor Biol.* (2018) 455:16–25. Available online at: https://linkinghub.elsevier.com/retrieve/pii/S0022519318303278 (Accessed June 6, 2025).
- 27. Rivera JN, Kierski TM, Kasoji SK, Abrantes AS, Dayton PA, Chang SX. Conventional dose rate spatially-fractionated radiation therapy (SFRT) treatment response and its association with dosimetric parameters—A preclinical study in a Fischer 344 rat model. *PloS One*. (2020) 15:e0229053. doi: 10.1371/journal.pone.0229053
- 28. Fernandez-Palomo C, Chang S, Prezado Y. Should peak dose be used to prescribe spatially fractionated radiation therapy?—A review of preclinical studies. *Cancers.* (2022) 14:3625. Available online at: https://www.ncbi.nlm.nih.gov/pmc/articles/PMC9330631/.
- 29. Tucker WW, Mazur TR, Schmidt MC, Hilliard J, Badiyan S, Spraker MB, et al. Script-based implementation of automatic grid placement for lattice stereotactic body radiation therapy. *Phys Imaging Radiat Oncol.* (2024) 29:100549. Available online at: https://linkinghub.elsevier.com/retrieve/pii/S2405631624000198 (Accessed June 6, 2025).
- 30. Gaudreault M, Chang D, Kron T, Siva S, Chander S, Hardcastle N, et al. Development of an automated treatment planning approach for lattice radiation therapy. *Med Phys.* (2024) 51:682–93. doi: 10.1002/mp.16761
- 31. Gaudreault M, Yu KK, Chang D, Kron T, Hardcastle N, Chander S, et al. Automated lattice radiation therapy treatment planning personalised to tumour size and shape. *Phys Med.* (2024) 125:104490. Available online at: https://linkinghub.elsevier.com/retrieve/pii/S1120179724002357 (Accessed June 6, 2025).
- 32. At B, Velayudham R. Assessing dosimetric advancements in spatially fractionated radiotherapy: From grids to lattices. *Med Dosim.* (2024) 49:206–14. Available online at: https://linkinghub.elsevier.com/retrieve/pii/S0958394723001164 (Accessed June 6, 2025).
- 33. Bhagyalakshmi AT, Ramasubramanian V. Impact of number and placement of high-dose vertices on equivalent uniform dose and peak-to-valley ratio for lattice radiotherapy. *J Med Phys.* (2024) 49:493–501. Available online at: https://www.ncbi.nlm.nih.gov/pmc/articles/PMC11801099/.
- 34. Yang D, Wang W, Hu J, Hu W, Zhang X, Wu X, et al. Feasibility of lattice radiotherapy using proton and carbon-ion pencil beam for sinonasal Malignancy. *Ann Transl Med.* (2022) 10:467. Available online at: https://www.ncbi.nlm.nih.gov/pmc/articles/PMC9096402/.
- 35. Halthore A, Fellows Z, Tran A, Deville C, Wright JL, Meyer J, et al. Treatment planning of bulky tumors using pencil beam scanning proton GRID therapy. *Int J Part Ther.* (2022) 9:40–9. Available online at: https://www.ncbi.nlm.nih.gov/pmc/articles/PMC9875826/.